The Journal of Immunology

RESEARCH ARTICLE | FEBRUARY 01 2022

SARS-CoV-2 NSP13 Inhibits Type I IFN Production by Degradation of TBK1 via p62-Dependent Selective Autophagy FREE

Chao Sui; ... et. al

J Immunol (2022) 208 (3): 753–761.
https://doi.org/10.4049/jimmunol.2100684

SARS-CoV-2 NSP13 Inhibits Type I IFN Production by Degradation of TBK1 via p62-Dependent Selective Autophagy

Chao Sui,*[,1] Tongyang Xiao,[†,‡,1] Shengyuan Zhang,[†,‡] Hongxiang Zeng,[†,‡] Yi Zheng,* Bingyu Liu,* Gang Xu,[†,‡] Chengjiang Gao,* and Zheng Zhang[†,‡,§,¶]

Severe acute respiratory syndrome coronavirus 2 (SARS-CoV-2), which causes coronavirus disease 2019 (COVID-19), has seriously threatened global public health. Severe COVID-19 has been reported to be associated with an impaired IFN response. However, the mechanisms of how SARS-CoV-2 antagonizes the host IFN response are poorly understood. In this study, we report that SARS-CoV-2 helicase NSP13 inhibits type I IFN production by directly targeting TANK-binding kinase 1 (TBK1) for degradation. Interestingly, inhibition of autophagy by genetic knockout of Beclin1 or pharmacological inhibition can rescue NSP13-mediated TBK1 degradation in HEK-293T cells. Subsequent studies revealed that NSP13 recruits TBK1 to p62, and the absence of p62 can also inhibit TBK1 degradation in HEK-293T and HeLa cells. Finally, TBK1 and p62 degradation and p62 aggregation were observed during SARS-CoV-2 infection in HeLa-ACE2 and Calu3 cells. Overall, our study shows that NSP13 inhibits type I IFN production by recruiting TBK1 to p62 for autophagic degradation, enabling it to evade the host innate immune response, which provides new insights into the transmission and pathogenesis of SARS-CoV-2 infection. ***The Journal of Immunology*****, 2022, 208: 753–761.**

The coronavirus disease 2019 (COVID-19) outbreak caused by severe acute respiratory syndrome coronavirus 2 (SARS-CoV-2) is raging across the world. SARS-CoV-2 is an enveloped, positive-sense, single-stranded RNA virus of the *Coronaviridae* family. Similar to other coronaviruses, SARS-CoV-2 contains a 29.7-kb genome, encoding a large polyprotein that is cleaved into 16 nonstructural proteins (NSP1–NSP16) by papain-like protease (NSP3) and 3C-like protease (NSP5), 4 structural proteins (S, E, M, and N), and 9 accessory proteins (3a, 3b, 6, 7a, 7b, 8, 9b, 9c, and 10) (1, 2). Most patients infected with SARS-CoV-2 are asymptomatic or have a mild syndrome, but some deteriorate to become severe cases or even die. Viremia and the impaired type I IFN (IFN-I) response have been reported to be associated with severe illness (3–5).

IFN is the first line of host defense against virus infection and is generally initiated by the recognition of pathogen-associated molecular patterns (6, 7). During SARS-CoV-2 infection, viral RNA is recognized by retinoic acid–inducible gene I (RIG-I)/melanoma differentiation gene 5 (MDA5) and activates the downstream MAVS/TANK-binding kinase 1 (TBK1)/IFN regulatory factor (IRF3) axis, initiating the expression of IFN-I (8–10). However, coronaviruses have evolved to develop multiple strategies to antagonize the host innate immune response. A number of SARS-CoV-2 proteins have been recently reported to antagonize the IFN-I response, such as papain-like protease (NSP3) (11, 12), 3C-like protease (NSP5) (11), ORF6 (13, 14), M protein (15), NSP1 (16), and N protein (17). Some of them directly interact with proteins associated with the IFN pathway to inhibit IFN production or the downstream JAK-STAT activation, but some are indirect. Autophagy hijacked by virus to degrade host proteins is another strategy to evade host immunity (18). The stability of adaptor proteins in the IFN-I signaling pathway can also be regulated by selective autophagy through cargo receptors, such as sequestosome 1 (SQSTM1/p62), CALCOCO2/NDP52, OPTN, and NBR1 (19–22).

In this study, we report a novel mechanism of how SARS-CoV-2 evades the host innate immune response through degradation of TBK1 on p62-dependent selective autophagy. SARS-CoV-2 NSP13 inhibits activity of the IFN-I pathway through forming a complex

*Key Laboratory of Infection and Immunity of Shandong Province, Department of Immunology, School of Basic Medical Sciences, Shandong University, Jinan, Shandong, China; [†]Institute of Hepatology, National Clinical Research Center for Infectious Disease, Shenzhen Third People's Hospital, Shenzhen, Guangdong Province, China; [‡]The Second Affiliated Hospital, School of Medicine, Southern University of Science and Technology, Shenzhen, Guangdong Province, China; [§]Shenzhen Research Center for Communicable Disease Diagnosis and Treatment of Chinese Academy of Medical Science, Shenzhen, Guangdong Province, China; and [¶]Guangdong Key laboratory for anti-infection Drug Quality Evaluation, Shenzhen, Guangdong Province, China

[1]C.S. and T.X. contributed equally to this work.

ORCIDs: 0000-0001-8483-2856 (T.X.); 0000-0002-3028-9007 (H.Z.); 0000-0003-0687-8108 (G.X.); 0000-0002-9365-4497 (C.G.).

Received for publication July 14, 2021. Accepted for publication November 22, 2021.

This work was supported by grants from the China National Funds for Distinguished Young Scholars (82025022 to Z.Z.), the National Natural Science Foundation of China (31730026 and 81930039 to C.G.), the Shenzhen Science and Technology Innovation Committee (KQTD20200909113758004, JSGG20200207155251653, and JSGG20200225151410198), the Central Charity Fund of the Chinese Academy of Medical Sciences (2020-PT310-009), the Bill & Melinda Gates Foundation, and by the Natural Science Foundation of Guangdong Province (2019A1515011072).

G.X., C.G., and Z.Z. conceived and designed research; C.S., T.X., G.X., and S.Z. performed research; H.Z., Y.Z., and B.L. provided discussions; C.S., T.X., G.X., C.G., and Z.Z. analyzed data; and C.S., T.X., G.X., C.G., and Z.Z. wrote the paper.

Address correspondence and reprint requests to Zheng Zhang, Chengjiang Gao, or Gang Xu, Institute of Hepatology, National Clinical Research Center for Infectious Disease, Shenzhen Third People's Hospital, Shenzhen 518112, Guangdong Province, China (Z.Z. and G.X.) or Key Laboratory of Infection and Immunity of Shandong Province, Department of Immunology, School of Basic Medical Sciences, Shandong University, Jinan, Shandong 250012, China (C.G.). E-mail addresses: zhangzheng1975@aliyun.com (Z.Z.), cgao@sdu.edu.cn (C.G.), or xugang2513@sina.com (G.X.).

The online version of this article contains supplemental material.

Abbreviations used in this article: Baf A1, bafilomycin A1; COVID-19, coronavirus disease 2019; CQ, chloroquine; HA, hemagglutinin; IFN-I, type I IFN; IRF3, IFN regulatory factor 3; IRSE, internal ribosome entry site; KO, knockout; MDA5, melanoma differentiation gene 5; MG132, carbobenzoxy-Leu-Leu-leucinal; MOI, multiplicity of infection; NSP, nonstructural protein; RIG-I, retinoic acid–inducible gene I; SARS-CoV-2, severe acute respiratory syndrome coronavirus 2; TBK1, TANK-binding kinase 1; VSV, vesicular stomatitis virus; WT, wild-type; ZBD, zinc-binding domain.

with TBK1 and p62. Overexpression of NSP13 or SARS-CoV-2 infection can induce p62 aggregation and then recruits TBK1 to the p62 complex. Our work reveals the potential of SARS-CoV-2 evading host antiviral immune responses and facilitating viral replication, providing insights into the prevention and treatment of COVID-19.

Materials and Methods

Reagents

Poly(I:C), carbobenzoxy-Leu-Leu-leucinal (MG132; C2211), chloroquine (CQ; C6628), and 3-methyladenine (3-MA; M9281) were purchased from Sigma-Aldrich and used at a final concentration of 1 μg/ml, 10 μM, 10 μM, and 10 mM, respectively. Bafilomycin A1 (Baf A1; tlrl-baf1) was purchased from InvivoGen and used at a final concentration of 1 μM. NSP13 inhibitors myricetin (HY-15097, MCE), bismuth (HY-B0796, MCE), scutellarein (HY-N0752, MCE), and SSYA10001 (HY-113794, MCE) were used at a final concentration of 10 μM. The Abs specific for TBK1 (38066), phospho-TBK1 (5483), and phospho-IRF3 (37829) were purchased from Cell Signaling Technology, and Abs specific for IRF3 were purchased from Invitrogen (39-2700). p62 (P0067) was from Sigma-Aldrich, STREP (A00875-40) was from GenScript, and hemagglutinin (HA, HT301-01), MYC (HT101-01), FLAG (HT201-01), ACTIN (HC201-01), and GAPDH (HC301-01) were from Transgen. The Abs specific for nucleoprotein of the SARS-CoV-2 were purchased from SinoBiological (40588-T62).

Cell culture

HEK-293T, HeLa, and HeLa-ACE2 cells were routinely cultured at 37°C with 5% CO_2 in DMEM (Life Technologies, 11965092) supplemented with 10% FBS (Life Technologies, 16140071) and 1% penicillin-streptomycin. Calu3 cells were cultured at 37°C with 5% CO_2 in MEM (Life Technologies, 11095080) supplemented with 20% FBS (Life Technologies, 16140071) and 1% penicillin-streptomycin. The p62 knockout (KO) HEK-293T cells and Beclin1 KO HEK-293T cells were generated by the CRISPR-Cas9 gene-editing system.

Virus and infection

Sendai virus was purchased from the China Center for Type Culture Collection (Wuhan University, China). Vesicular stomatitis virus (VSV) was provided by Prof. H. Meng (Institute of Basic Medicine, Shandong Academy of Medical Sciences, China). For VSV and Sendai virus infection, HEK-293T cells were infected with virus at a multiplicity of infection (MOI) of 1 at indicated time points.

All studies involving SARS-CoV-2 infection were conducted in the biosafety level-3 laboratory of Shenzhen Third People's Hospital. The SARS-CoV-2 SZTH-003 was isolated from samples of a COVID-19 patient using Vero-E6 cells. The genomic sequence of SZTH-003 has been deposited in the Global Initiative of Sharing All Influenza Data (EPI_ISL_406594). Titration of SARS-CoV-2 was performed on Vero-E6 cells by a plaque assay. SARS-CoV-2 stocks used in this study had undergone four passages on Vero-E6 cells and were stored at −80°C. Calu3 or HeLa-ACE2 cells were infected with virus at an MOI of 1 at the indicated time points. After adsorption for 1 h at 37°C, the cells were washed with PBS and cultured in normal media.

Confocal microscopy

HeLa, HeLa-ACE2, or Calu3 cells were cultured on coverslips and infected with SARS-CoV-2 for 24 h, then washed with PBS (Takara, T900) and fixed in 4% paraformaldehyde for 30 min at room temperature. After washing with PBS, cells were permeabilized with 0.5% Triton X-100 (Sangon Biotech, A110694) in PBS at room temperature for 20 min, and then washed with PBS again. The cells were blocked with 5% BSA (Beyotime, ST025) for 1 h followed by incubation with the appropriate primary Ab at 4°C overnight. On the next day, the cells were incubated with fluorescent-labeled secondary Abs. Nuclei were stained with DAPI (Beyotime, C1102). Following staining, the stained cells were examined under a Leica DMi8 laser confocal microscopy (Leica Microsystems). Pearson's correlation coefficient for colocalization was analyzed by a colocalization finder plugin of ImageJ.

Quantitative real-time PCR

RNA was isolated from the indicated cells by using TRIzol reagent (Invitrogen, 15596018), and a fifth volume of chloroform was added to the lysate and shaken violently for 15 s before centrifugation at 12,000 × *g* at 4°C for 15 min. An equal volume of precooled isopropyl alcohol was added and mixed upside down after careful absorption of the upper aqueous phase into a new centrifuge tube. Then, it was left for 10 min at 4°C and centrifuged at 12,000 × *g* at 4°C for 10 min. The supernatant was removed, and 1 ml of 75% ethanol was added. The samples were centrifuged at 12,000 × *g* at 4°C for 5 min, with its supernatant being discarded. An appropriate amount of RNase-free double-distilled H_2O was added to dissolve the RNA.

Total RNA was then reverse transcribed with a quantitative reverse transcription kit (Takara, RR047A). Quantitative real-time PCR was carried out in triplicate using SYBR Green (Vazyme, Q311) according to the manufacturer's instructions, and fold changes were calculated with the $2^{-\Delta\Delta Ct}$ method, where ΔCt is the difference between the amplification fluorescence threshold of the mRNA of interest and the mRNA of *gapdh* used as the internal reference. Primers for IFN-β were 5′-CAGCAATTTTCAGTGTCAGAAGC-3′ (forward) and 5′-TCATCCTGTCCTTGAGGCAGT-3′ (reverse), and for *gapdh* were 5′-ACAACTTTGGTATCGTGGAAGG-3′ (forward) and 5′-GCCATCACGCCACAGTTTC-3′ (reverse).

Immunoprecipitation and immunoblotting

For immunoblotting, whole-cell lysates were prepared by lysing the cells for 15 min at 4°C in 2× SDS loading buffer [100 mM Tris-HCl (pH 6.8), 200 mM DTT, 4% SDS, 0.2% bromophenol blue, 20% glycerol]. For immunoprecipitation, whole-cell lysates were prepared by lysing the cells for 30 min at 4°C in Nonidet P-40 buffer [50 mM Tris-HCl (pH 7.4), 150 mM NaCl, 10% glycerol, 0.5% Nonidet P-40, 1 mM NaF] containing 1 mM PMSF (Solarbio Life Sciences) and a protease inhibitor mixture (Sigma, P8340). Lysates were centrifuged at 12,000 × *g* for 10 min at 4°C. Immunoprecipitation was performed using mouse anti-FLAG, anti-MYC, or anti-HA Abs with protein A/G agarose beads (Thermo Scientific, 22852).

Western blotting of the cell lysates and immunoprecipitates was performed using mouse anti-FLAG, anti-HA, anti-MYC, anti-STREP, and other Abs as indicated. Immunoblot analysis was also performed on equal amounts of proteins, and signals were developed with the SuperSignal West Pico PLUS chemiluminescent substrate (Thermo Scientific, 34580).

Luciferase reporter assay

For the IRF3 or IFN-stimulated regulatory element luciferase reporter assay, the cells were transfected with plasmids encoding the IRF3 or IFN-stimulated regulatory element luciferase reporter gene and indicated plasmids in 96-well plates. After 24 h of transfection, the cells were collected and lysed. Luciferase activity was measured with the Bright-Glo luciferase assay system (Promega, E2620) according to the manufacturer's protocols. Briefly, 100 μl of reagent was added to cells grown in 100 μl of medium, and luminescence was measured after the completion of cell lysis.

For the IFN-β luciferase reporter assay, the cells were transfected with IFN-β luciferase reporter plasmid and the indicated plasmids, and luciferase activity was measured with the Dual-Luciferase reporter assay system (Promega, E2620) according to the manufacturer's protocols. Data were normalized by the ratio of firefly to *Renilla* luciferase activity.

Statistical analysis

Statistically significant differences between groups and treatments were determined by one-way ANOVA, and those between groups were determined by the Tukey multiple comparison test or Student *t* test using GraphPad Prism 8.3 software. A p value <0.05 was considered statistically significant.

Results

SARS-CoV-2 NSP13 inhibits expression of IFN-I

Previous screening showed that SARS-CoV-2 NSP13 significantly inhibited the poly(I:C)-induced IFN production (13). To further confirm the data, HEK-293T cells were transfected with NSP13 or empty vector for 24 h, then infected with VSV at the designated time points. The mRNA level of IFN-β was quantified by quantitative real-time PCR. While VSV infection could induce strong IFN-β expression, a significant reduction of IFN-β had been observed in the presence of NSP13 (Fig. 1A). To further study the antagonistic effect of SARS-CoV-2 NSP13 on IFN-I, activation of the IFN-β promoter induced by RIG-I, MDA5, MAVS, TBK1, and IRF3 was detected in HEK-293T cells transfected with NSP13 expressing plasmid or empty vector. The results showed that the IFN-β luciferase reporter activity was significantly suppressed by NSP13 in HEK-293T cells with RIG-I, MDA5, MAVS, or TBK1 expression, but it was not affected in HEK-293T cells with IRF3 expression (Fig. 1B). Furthermore, the expression of NSP13 impaired IRF3 luciferase reporter and internal ribosome entry site (IRSE) promoter activity induced by TBK1 in

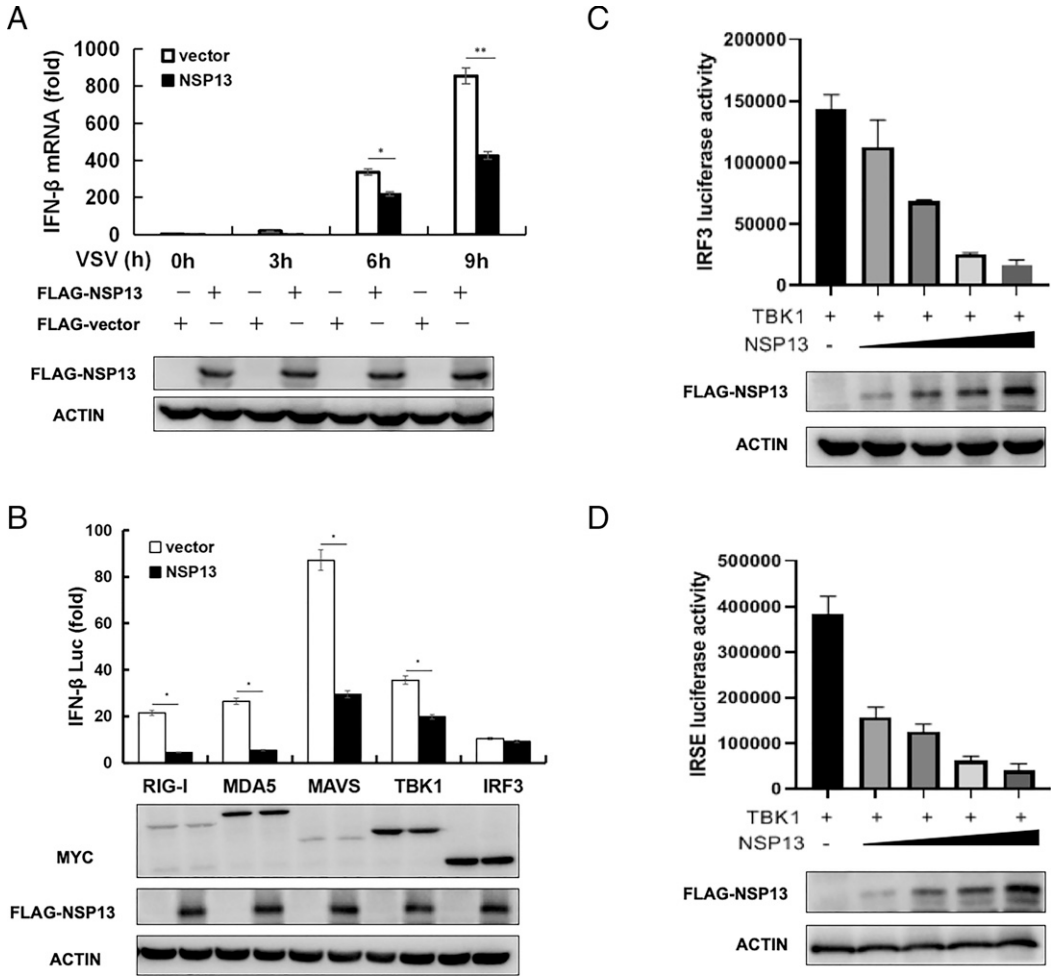

FIGURE 1. SARS-CoV-2 NSP13 inhibits IFN production. (**A**) HEK-293T cells transfected with NSP13 or empty vector were infected with VSV at the designated time points. Quantitative real-time PCR was performed to measure the mRNA level of IFN-β. Whole-cell lysates were immunoblotted with anti-FLAG and anti-ACTIN ($n = 3$ independent experiments). (**B**) Luciferase assay of HEK-293T cells transfected with the IFN-β reporter plasmids together with MYC-tagged RIG-I, MDA5, MAVS, TBK1, or IRF3 with or without the NSP13 expression plasmid. The immunoblot was analyzed with anti-FLAG, anti-MYC, or anti-ACTIN Ab ($n = 3$ independent experiments). IFN-β Luc, IFN-β luciferase reporter. (**C**) The IRF3 luciferase reporter assay was evaluated in HEK-293T cells cotransfected with TBK1, IRF3 reporter plasmids, and different doses of NSP13 (0, 0.025, 0.05, 0.10, and 0.125 μg, respectively). The immunoblot was analyzed with anti-FLAG or anti-ACTIN Ab ($n = 3$ independent experiments). (**D**) The promoter activity of IRSE was evaluated in HEK-293T cells cotransfected with TBK1, IRSE luciferase reporter plasmids, and different doses of NSP13 (0, 0.025, 0.05, 0.10, and 0.125 μg, respectively). The immunoblot was analyzed with anti-FLAG or anti-ACTIN Ab ($n = 3$ independent experiments). All quantitative real-time PCR data are normalized to the *gapdh* gene. The control group is used as a reference. The error bars represent the SD, and differences between the experimental and control groups were determined by one-way ANOVA (*$p < 0.05$, **$p < 0.01$).

a dose-dependent manner (Fig. 1C, 1D). These results suggest that NSP13 can inhibit the production of IFN induced by viral infection and act upstream of IRF3.

SARS-CoV-2 NSP13 interacts with TBK1

A previous study on the SARS-CoV-2–host interaction suggested a possible interaction between NSP13 and TBK1 (23), which is an important kinase for regulation of IFN generation. To confirm the interaction of TBK1 and NSP13, FLAG-NSP13 and HA-TBK1 were cotransfected into HEK-293T cells, and the TBK1 complex was pulled down by immunoprecipitation with anti-HA Ab. FLAG-NSP13 was detected in TBK1 immunoprecipitates (Fig. 2A), and HA-TBK1 could also be detected in FLAG-NSP13 immunoprecipitates (Fig. 2B). In addition, the colocalization of NSP13 and TBK1 was also observed in HeLa cells cotransfected with FLAG-NSP13 and HA-TBK1 (Fig. 2C–E, Supplemental Fig. 1). These data show that SARS-CoV-2 NSP13 interacts with TBK1, the key kinase that regulates the IFN signaling pathway.

SARS-CoV-2 NSP13 promotes autophagic degradation of TBK1

To explore the mechanism of NSP13 inhibiting IFN-I production, we detected the phosphorylation of TBK1 and IRF3 in vector- or NSP13-transfected HEK-293T cells infected with VSV. The immunoblot results showed that the phosphorylation of endogenous TBK1 and IRF3 was induced by VSV infection in cells transfected with empty vector, but it was significantly impaired by the presence of NSP13 (Fig. 3A). Unexpectedly, the total TBK1 decreased in HEK-293T cells with overexpression of NSP13 with or without VSV infection, whereas the level of IRF3 was not impaired (Fig. 3A). In NSP13 and TBK1 cotransfected HEK-293T cells, the level of TBK1 was also decreased (Fig. 3B). The overexpression TBK1 has strong autophosphorylation and can phosphorylate IRF3, but phosphorylation of both TBK1 and IRF3 was found to be diminished by NSP13

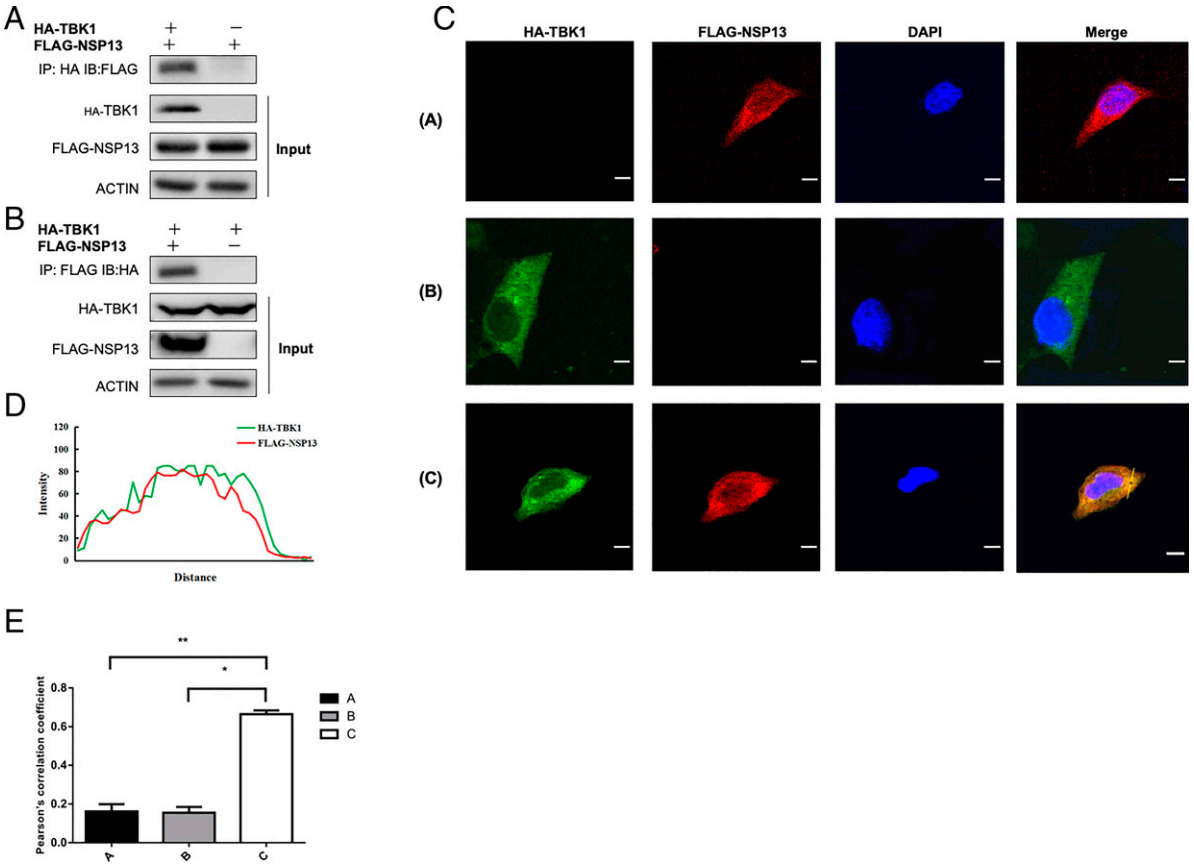

FIGURE 2. SARS-CoV-2 NSP13 interacts with TBK1. (**A** and **B**) HEK-293T cells were transfected with vectors encoding HA-TBK1 and FLAG-NSP13, followed by coimmunoprecipitation with anti-HA (A) or anti-FLAG (B) Ab and immunoblot analysis with anti-FLAG or anti-HA Ab ($n = 2$ independent experiments). (**C**) Confocal microscopy of HeLa cells transfected with vectors encoding HA-TBK1 and FLAG-NSP13. Immunofluorescence was performed using anti-HA (green) and anti-FLAG (red) Abs and DAPI (blue). Scale bars, 10 μm ($n = 2$ independent experiments). (**D**) Intensity profiles of NSP13 and TBK1 along the plotted lines in (C), as analyzed by ImageJ line scan analysis. (**E**) Pearson's correlation coefficient for TBK1 and NSP13 colocalization was analyzed by the colocalization finder plugin of ImageJ. The error bars represent the SD, and differences between the experimental and control groups were determined by one-way ANOVA ($*p < 0.05$, $**p < 0.01$).

(Fig. 3B). We also tested the effects of NSP13 on other critical adaptors in the IFN-I pathway and found that the levels of RIG-I, MDA5, MAVS, and IRF3 were not decreased upon NSP13 overexpression (Supplemental Fig. 2). These data suggest that NSP13 specificity reduces TBK1 protein level, thus destroying the TBK1/IRF3 axis and reducing IFN transcription.

The control of protein degradation in eukaryotic cells relies on two major systems including the ubiquitin–proteasome pathway and the autophagy–lysosome pathway (24). We then wondered which pathway contributed to SARS-CoV-2 NSP13-mediated TBK1 degradation. HEK-293T cells were cotransfected with FLAG-NSP13 and HA-TBK1 plasmids and then treated with autophagy inhibitor or proteasome inhibitor. Immunoblot analysis revealed that degradation of TBK1 was rescued by autophagy inhibitors 3-MA, CQ, and BafA1 rather than the proteasome inhibitor MG132 (Fig. 3C). To further assess the importance of autophagy in this process, NSP13 and TBK1 were cotransfected into Beclin1 KO HEK-293T cells and wild-type (WT) HEK-293T cells. The TBK1 degradation induced by NSP13 was in a dose-dependent manner in WT HEK-293T cells, but it was completely abolished in Beclin1 KO cells (Fig. 3D). These data indicate that NSP13-mediated TBK1 degradation is dependent on autophagy but not proteasome.

Surprisingly, LC3II/LC3I did not increase in NSP13-overexpressing cells (Fig. 3B), and NSP13 also did not interact with the autophagy regulator VSP34 complex (Vps34, Beclin1, and Uvrag) (Supplemental Fig. 3A). However, the colocalization of TBK1 with LC3 was increased in NSP13-expressed HeLa cells (Supplemental Fig. 3B, 3C). These data suggest that the NSP13 does not directly induce autophagy but promotes TBK1 recruitment into autophagosome.

To further confirm that NSP13 inhibits IFN production depending on autophagic degradation of TBK1, Beclin1 KO HEK-293T cells were transfected with NSP13 or vector and then infected with VSV at the indicated time points. The mRNA level of IFN-β induced by VSV was not significantly reduced after NSP13 transfection in autophagy deficient cells (Fig. 3E). Consistently, the IFN-β luciferase reporter activity was not significantly suppressed by NSP13 in Beclin1 KO HEK-293T cells with RIG-I, MDA5, MAVS, TBK1, and IRF3 expression (Fig. 3F).

NSP13, as the helicase-regulated SARS-CoV-2 replication, has ATP hydrolysis activity and dsDNA unwinding activity (25). To explore whether the ATP hydrolysis activity and dsDNA unwinding activity of NSP13 regulated degradation of TBK1, the inhibitors of ATP hydrolysis activity (myricetin and scutellarein) and dsDNA unwinding activity (bismuth and SSYA10001) were both used to treat NSP13 and TBK1 coexpressing HEK-293T cells. The level of TBK1 was still decreased in myricetin, scutellarein, or bismuth and SSYA10001-treated HEK-293T cells (Supplemental Fig. 3D). These results indicate that the autophagic degradation of TBK1 is independent on the ATP hydrolysis activity and dsDNA unwinding activity of NSP13.

SARS-CoV-2 NSP13 induces selective autophagic degradation of TBK1 by interacting with p62

To identify the cargo receptors involved in NSP13-mediated TBK1 degradation, we sought to use affinity purification mass spectrometry

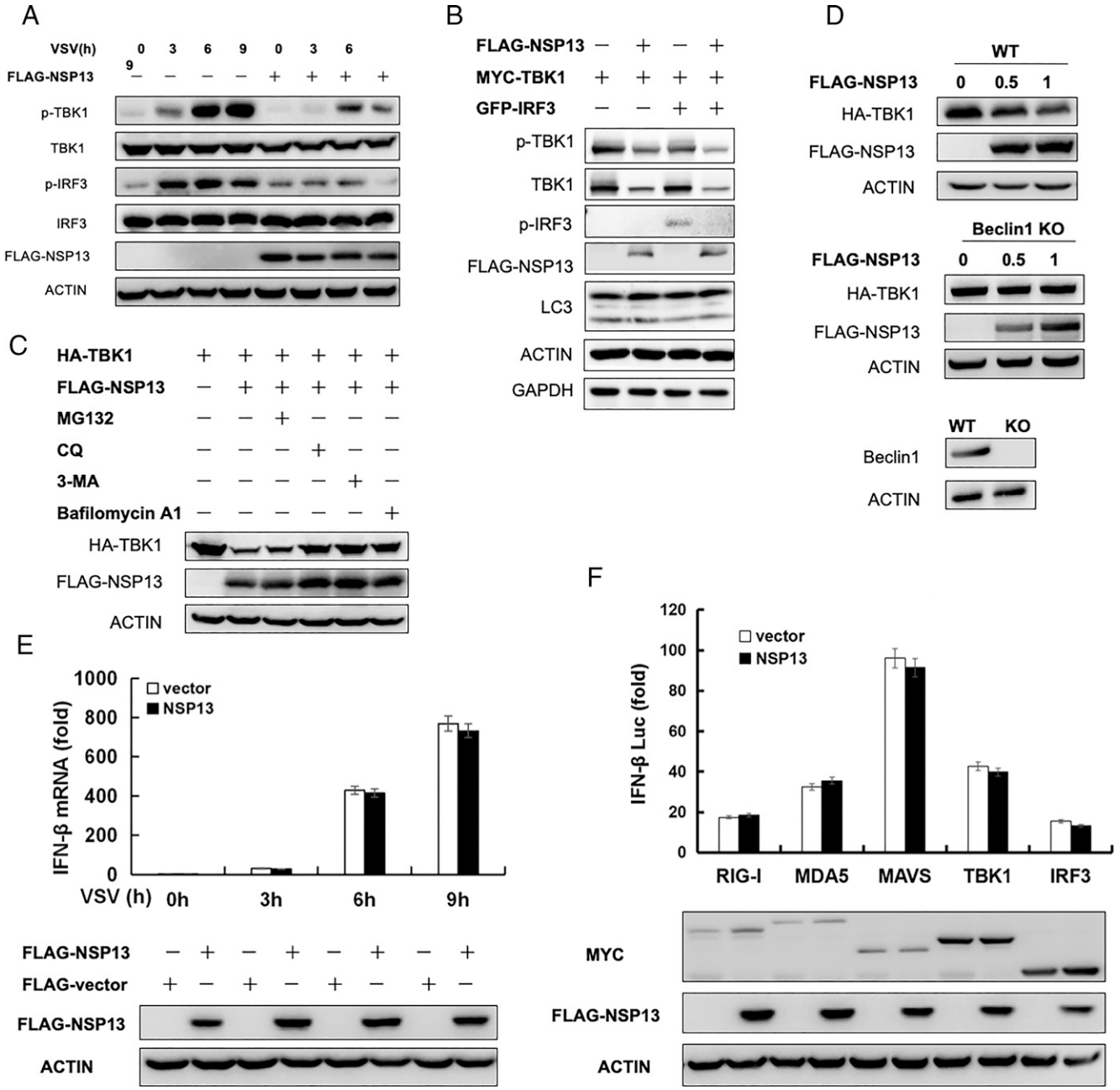

FIGURE 3. SARS-CoV-2 NSP13 degrades TBK1 by the RIG-I–like receptor pathway. (**A**) HEK-293T cells were transfected with or without FLAG-NSP13 and infected with VSV at the designated time points. Endogenous TBK1 and IRF3 were immunoblotted ($n = 2$ independent experiments). (**B**) HEK-293T cells were transfected with FLAG-NSP13, MYC-TBK1, and GFP-IRF3 plasmids for 24 h. The total cell lysates were immunoblotted for TBK1, IRF3, and endogenous LC3 ($n = 2$ independent experiments). (**C**) HEK-293T cells were transfected with FLAG-NSP13 and MYC-TBK1 and then treated with 10 μM MG132, 10 μM CQ, 10 mM 3-MA, or 1 μM Baf A1 for 6 h before harvest. TBK1 and NSP13 were immunoblotted ($n = 2$ independent experiments). (**D**) Immunoblotting analysis of HA-TBK1 in cell lysates of WT and Beclin1 KO cells transfected with different doses of FLAG-NSP13 ($n = 2$ independent experiments). (**E**) Beclin1 KO HEK-293T cells transfected with NSP13 or empty vector were infected with VSV at the designated time points, and quantitative real-time PCR was performed to measure the mRNA level of IFN-β. Whole-cell lysates were immunoblotted with anti-FLAG and anti-ACTIN ($n = 3$ independent experiments). (**F**) Luciferase assay of Beclin1 KO HEK-293T cells transfected with the IFN-β reporter plasmids together with MYC-tagged RIG-I, MDA5, MAVS, TBK1, or IRF3 with or without the NSP13 expression plasmid. Immunoblot analysis included anti-FLAG, anti-MYC, or anti-ACTIN Ab ($n = 3$ independent experiments). All quantitative real-time PCR data are normalized to the *gapdh* gene. The control group is used as a reference. Error bars represent the SD. IFN-β Luc, IFN-β luciferase reporter.

to identify the NSP13 binding proteins. FLAG-NSP13 was transfected into HeLa and HeLa-ACE2 cells, and the NSP13 complex was pulled down by immunoprecipitation with anti-FLAG Ab. The precipitation was subjected to SDS-PAGE and stained with Coomassie blue, followed by detection of protein mass spectrometry (Fig. 4A). The analysis revealed that SQSTM1/p62 peptides were enriched in the NSP13 immunoprecipitation group rather than in the vector group (Fig. 4B), which indicated the potential of p62 to act as a candidate cargo receptor. A previous study reported that p62 acted as the cargo receptor in a variety of virus infections to selectively degrade host proteins (20). To determine whether TBK1 degradation was regulated by p62-mediated selective autophagy, we cotransfected NSP13 and TBK1 into p62 KO HEK-293T cells and found that the absence of p62 effectively rescued NSP13-mediated

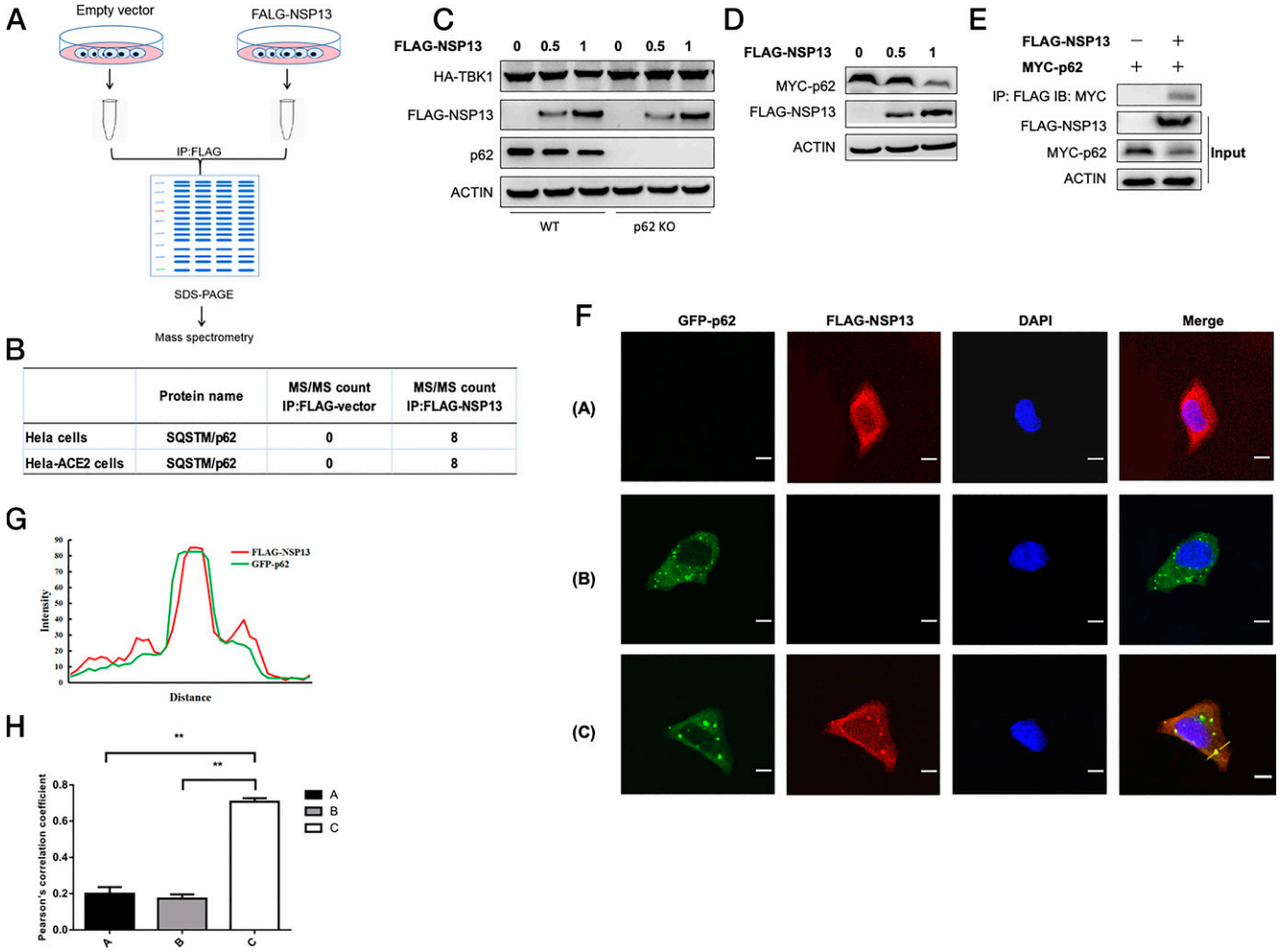

	Protein name	MS/MS count IP:FLAG-vector	MS/MS count IP:FLAG-NSP13
Hela cells	SQSTM/p62	0	8
Hela-ACE2 cells	SQSTM/p62	0	8

FIGURE 4. SARS-CoV-2 NSP13 interacts with p62. (**A**) FLAG-NSP13 was transfected into HeLa and HeLa-ACE2 cells. Then NSP13 complex was pulled down by immunoprecipitation with anti-FLAG Ab. The precipitation was subjected to SDS-PAGE and stained with Coomassie Blue, followed by analysis using protein mass spectrometry. (**B**) Significant p62 enriched in NSP13 immunoprecipitates by quantitative mass spectrometry ($n = 3$ independent experiments). (**C**) Immunoblotting analysis of HA-TBK1 in cell lysates of WT and p62 KO HEK-293T cells transfected with different doses of FLAG-NSP13 ($n = 2$ independent experiments). (**D**) HEK-293T cells were transfected with FLAG-NSP13 and different doses of MYC-p62 plasmids for 24 h. p62 and NSP13 were immunoblotted ($n = 2$ independent experiments). (**E**) HEK-293T cells were transfected with vectors encoding MYC-p62 and FLAG-NSP13, followed by coimmunoprecipitation with anti-FLAG Ab and immunoblot analysis with anti-MYC Ab ($n = 2$ independent experiments). (**F**) Confocal microscopy of HeLa cells were transfected with FLAG-NSP13 and GFP-p62, and the immunofluorescence was performed using anti-FLAG (red) Abs, GFP (green), and DAPI (blue). Scale bars, 10 μm ($n = 2$ independent experiments). (**G**) Intensity profiles of NSP13 and p62 along the plotted lines in Figure 4F, as analyzed by ImageJ line scan analysis. (**H**) Pearson's correlation coefficient for p62 and NSP13 colocalization was analyzed by the colocalization finder plugin of ImageJ. Error bars represent the SD, and differences between the experimental and control groups were determined by one-way ANOVA (**$p < 0.01$).

TBK1 degradation (Fig. 4C). More interestingly, the overexpression of NSP13 induced degradation of endogenous and exogenous p62 in a dose-dependent manner (Fig. 4C, 4D). Meanwhile, p62 interaction with NSP13 was confirmed in HEK-293T cells that were cotransfected with FLAG-NSP13– and MYC-p62–expressing plasmids (Fig. 4E). Immunofluorescence analysis further revealed that NSP13 colocalized with p62 (Fig. 4F–H, Supplemental Fig. 4A).

Although TBK1 does not interact directly with p62, it can be detected in p62 immunoprecipitates in the presence of NSP13 (Fig. 5A). The immunofluorescence analysis also revealed that TBK1 colocalized with p62 only in cells with overexpression of NSP13 (Fig. 5B–D, Supplemental Fig. 4B). These data suggested that SARS-CoV-2 NSP13 acted as a bridge to recruit TBK1 and p62 to form TBK1–NSP13–p62 complexes. To explore which domain of NSP13 was responsible for the interaction with TBK1 and p62, the N-terminal zinc-binding domain (ZBD) and C-terminal "RecA-like" domain truncation variants were constructed. An immunoprecipitation assay showed that p62 was bound to both the ZBD and RecA domains except the full-length NSP13, but the ZBD domain showed a stronger interaction with p62 (Fig. 5E). TBK1 only interacted with full-length NSP13 and the RecA domain (Fig. 5F), indicating that NSP13 recruits TBK1 by its RecA domain. These data suggested that p62 mainly bonded to the ZBD domain of NSP13, and TBK1 mainly interacted with the RecA domain of NSP13 to form TBK1–NSP13–p62 complexes (Fig. 5G).

SARS-CoV-2 infection degrades TBK1 and induces p62 aggregation

To explore whether TBK1 is degraded during SARS-CoV-2 infection, Calu3 cells were infected with 1 MOI of SARS-CoV-2 at different time points. Immunoblotting of viral nucleocapsid showed that SARS-CoV-2 replication was markedly enhanced along with time (Fig. 6A). Unlike a previous study (26), we found that SARS-CoV-2 infection induced strong phosphorylation of TBK1 in Calu3 cells at 8–24 h postinfection (Fig. 6A). Endogenous TBK1 and p62 were significantly reduced at 8 h after viral infection and then recovered (Fig. 6A). The viral proteins were

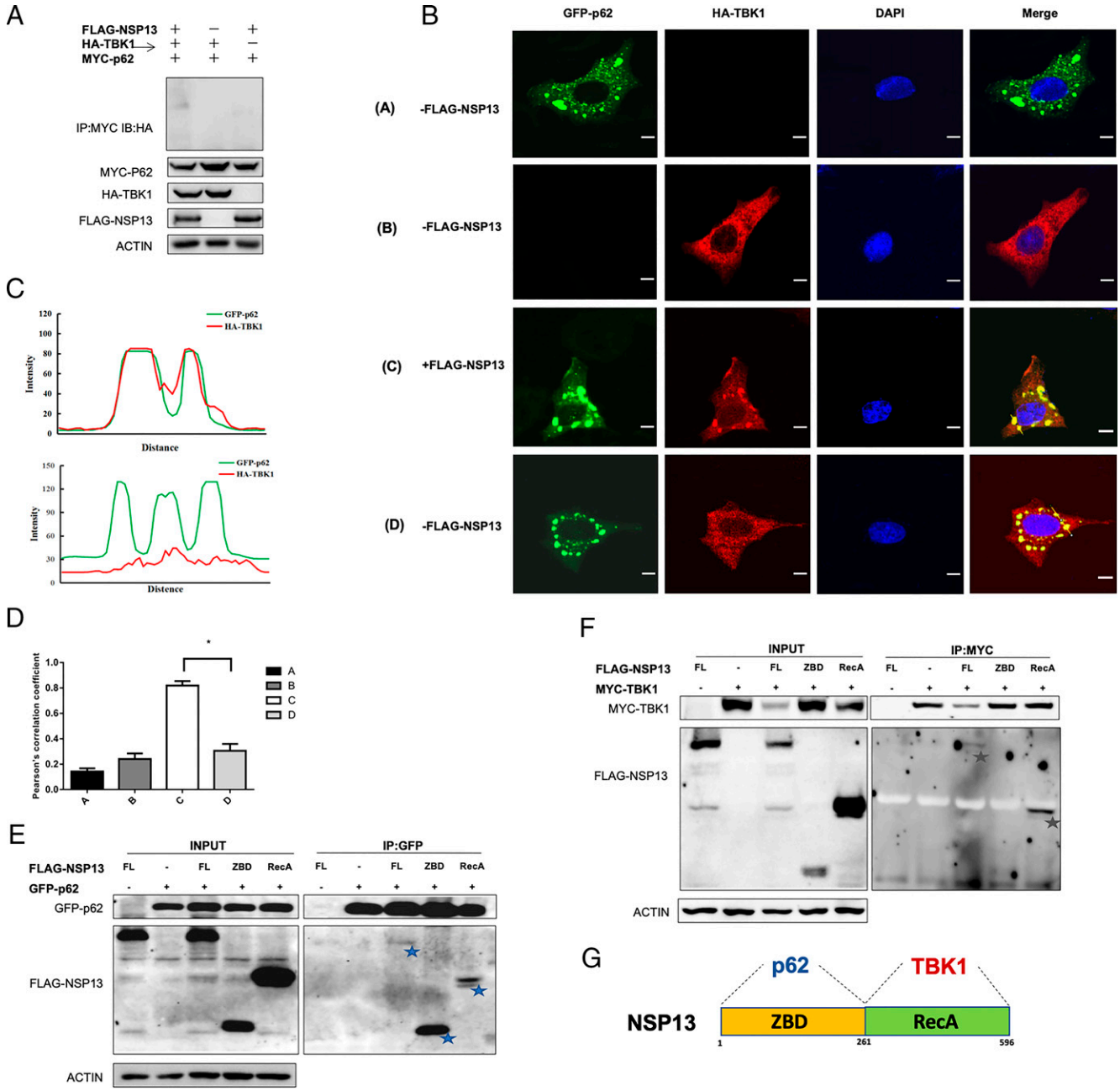

FIGURE 5. NSP13 interacts with p62 and TBK1 by different domains. (**A**) HEK-293T cells were transfected with vectors encoding MYC-p62, HA-TBK1, and FLAG-NSP13, followed by coimmunoprecipitation with anti-MYC Ab and immunoblot analysis with anti-HA and anti-FLAG Ab ($n = 2$ independent experiments). (**B**) Confocal microscopy of HeLa cells transfected with GFP-p62 and HA-TBK1 with or without FLAG-NSP13. Immunofluorescence was performed using anti-HA (red) Abs, GFP (green), and DAPI (blue). Scale bars, 10 μm ($n = 2$ independent experiments). (**C**) Intensity profiles of p62 and TBK1 with or without FLAG-NSP13 along the plotted lines in Fig. 4H, as analyzed by ImageJ line scan analysis. (**D**) Pearson's correlation coefficient for p62 and TBK1 colocalization with or without FLAG-NSP13 was analyzed by the colocalization finder plugin of ImageJ. Error bars represent the SD, and differences between the experimental and control groups were determined by one-way ANOVA ($*p < 0.05$). (**E**) HEK-293T cells were transfected with FLAG-NSP13, indicated truncated NSP13, and GFP-p62 plasmids for 24 h, followed by coimmunoprecipitation with anti-GFP Ab and immunoblot analysis with anti-FLAG Ab ($n = 2$ independent experiments). (**F**) HEK-293T cells were transfected with FLAG-NSP13, indicated truncated NSP13, and MYC-TBK1 plasmids for 24 h, followed by coimmunoprecipitation analysis with anti-MYC Ab and immunoblot analysis with anti-FLAG Ab. Blue star represents full-length or truncated NSP13 interacting with p62; gray stars represent full-length or truncated NSP13 interacting with TBK1 ($n = 2$ independent experiments). (**G**) Schematic diagram of NSP13 interacting with p62 and TBK1 by different domains.

highly expressed after 16 h of infection, and SARS-CoV-2 ORF3a was reported to inhibit autophagic flux (27). This may promote the recovery of TBK1 and p62 levels in the postinfection period.

Furthermore, confocal microscopy analysis was performed to explore the effect of p62 on SARS-CoV-2 replication. HeLa-ACE2 cells were infected with SARS-CoV-2, and infection efficiency was detected by immunostaining of viral nucleocapsid. Confocal microscopy analysis demonstrated the enhanced aggregates of p62 in SARS-CoV-2–infected cells, which suggested that p62 performed as an important autophagy cargo receptor in delivering proteins to autophagosome during SARS-CoV-2 infection

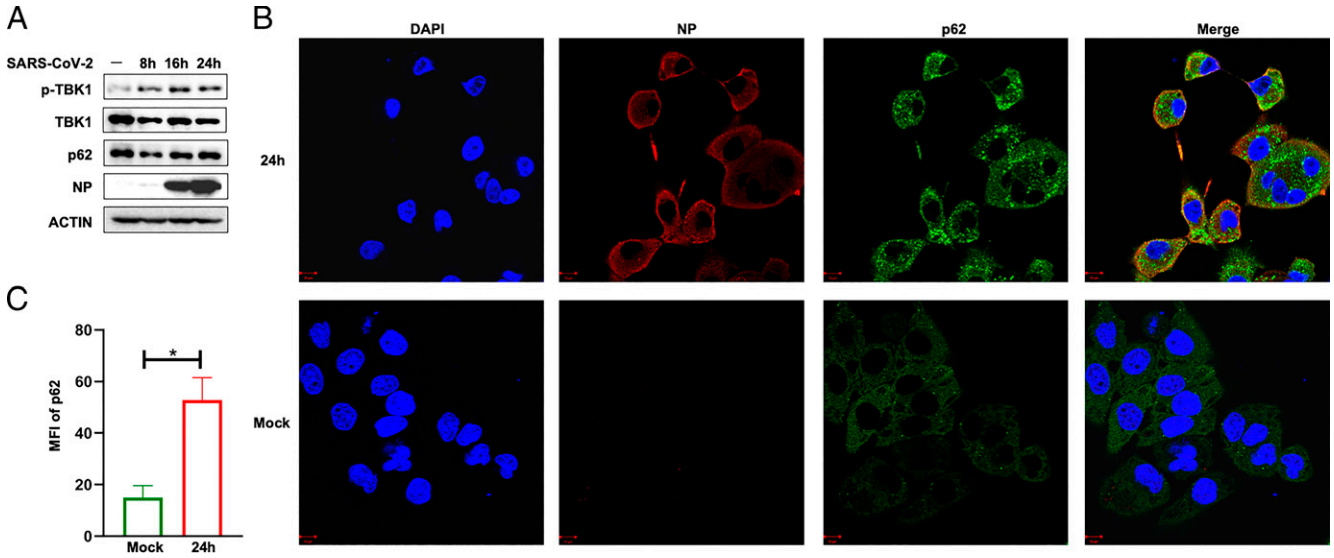

FIGURE 6. SARS-CoV-2 infection degrades TBK1 and induces p62 aggregation. (**A**) Immunoblot analysis of the indicated proteins in lysates of Calu3 cells infected with SARS-CoV-2 for 8, 16, and 24 h ($n = 2$ independent experiments). (**B**) Confocal microscopy of HeLa-ACE2 cells infected with SARS-CoV-2 for 24 h. Immunofluorescence was performed using anti-nucleoprotein (NP) (red) and anti-p62 (green) Abs and DAPI (blue). Scale bars, 10 μm ($n = 2$ independent experiments). (**C**) The mean fluorescence intensity (MFI) of p62 from immunofluorescence upon SARS-CoV-2 infection for 24 h in HeLa-ACE2 cells ($n = 2$ independent experiments). Experiments were calculated as the means. Error bars represent the SD, and differences between the experimental and control groups were determined by an unpaired *t* test ($*p < 0.05$).

(Fig. 6B, 6C). Collectively, these data reveal that SARS-CoV-2 infection is able to suppress IFN-I pathway by p62-depended selective autophagic degradation of TBK1.

Discussion

Previous studies have reported that host antiviral immune responses play a critical role in fighting against SARS-CoV-2 infection (28). The antagonistic mechanism of antiviral innate immunity by SARS-CoV-2 may be the cause of death in COVID-19 patients (26, 29, 30). The SARS-CoV-2 proteins that antagonize IFN-I and IFN-stimulated gene production have been identified (11, 12, 15, 30). Although previous studies have identified NSP13 as inhibiting IFN production, and some found that NSP13 interacted with TBK1 and inhibited the phosphorylation of TBK1 and IRF3 (13, 31–33), the detailed mechanism was unknown. Here, we found that SARS-CoV-2 NSP13 recruited TBK1 to p62 for degradation, thus inhibiting IFN-I generation.

TBK1 is an important adaptor in the induction of IFN-I and proinflammatory cytokines activated by RNA and DNA viruses. There are multiple mechanisms that affect the IFN-I pathway by regulating TBK1 activity. DExD/H-box RNA helicase 19 (DDX19), E3 ubiquitin ligase DTX4, TRAF-interacting protein (TRIP)13, deubiquitinating enzymes CYLD and USP2b, and ubiquitin-conjugating enzyme 2S (UBE2S) promote the degradation of TBK1 to inhibit IFN-I production (34–39), whereas E3 ubiquitin ligase MIB1, MIB2, Nrdp1, and RNF128 increase the level of K63-linked ubiquitination of TBK1 to enhance activity of IFN-I (40–42). Furthermore, other viral proteins are reported to downregulate TBK1-dependent antiviral innate immunity. The tegument protein UL46 of HSV-1 interacts with TBK1 and inhibits its dimerization, thus reducing IFN-I production (43). The SARS-CoV-2 membrane protein induces TBK1 degradation via K48-linked ubiquitination (44). Our data highlighted that TBK1 colocalized to and interacted with SARS-CoV-2 NSP13, which was consistent with the results of NSP13-targeted affinity purification mass spectrometry (23). We found that NSP13 reduced phosphorylation of TBK1 and downregulated TBK1 protein level. In addition, SARS-CoV-2 NSP13 helicase is an important component for viral replication and is able to hydrolyze NTPs and destabilize RNA helix (45). We provide evidence that the process of SARS-CoV-2 NSP13 inhibiting the IFN-I pathway regulated by TBK1 was independent of its NTPase and RNA helicase activities.

Importantly, we found that the degradation of TBK1 was rescued by autophagy inhibitors rather than by proteasome inhibitors. In Beclin1 and p62 KO HEK-293T cells, TBK1 was not degraded despite the overexpression of SARS-CoV-2 NSP13, indicating that SARS-CoV-2 NSP13 promoted TBK1 degradation in an autophagy-dependent manner. We further assessed the role of p62 in the degradation of TBK1 induced by SARS-CoV-2 NSP13, an important cargo receptor in selective autophagy. Many adaptors in the IFN-I pathway and inflammatory response are regulated by autophagic cargo receptor p62, such as stimulator of IFN genes (STING) and absent in melanoma 2 (AIM2) (46, 47). We found that p62 expression was reduced by SARS-CoV-2 NSP13 in a dose-dependent manner. Interaction and colocalization exist between p62 and SARS-CoV-2 NSP13. The authentic SARS-CoV-2 infection further supports the conclusion that TBK1 and SARS-CoV-2 NSP13 form a p62-associated complex that enters autophagosome to degrade TBK1 after fusing with lysosome. Altogether, our work demonstrates that SARS-CoV-2 NSP13 antagonizes host antiviral innate immunity by p62-dependent selective autophagic degradation of TBK1. These findings may provide the optimal therapeutic strategies based on selective autophagy for COVID-19 patients.

Disclosures

The authors have no financial conflicts of interest.

References

1. Ren, L. L., Y. M. Wang, Z. Q. Wu, Z. C. Xiang, L. Guo, T. Xu, Y. Z. Jiang, Y. Xiong, Y. J. Li, X. W. Li, et al. 2020. Identification of a novel coronavirus causing severe pneumonia in human: a descriptive study. *Chin. Med. J. (Engl.)* 133: 1015–1024.
2. Marra, M. A., S. J. M. Jones, C. R. Astell, R. A. Holt, A. Brooks-Wilson, Y. S. N. Butterfield, J. Khattra, J. K. Asano, S. A. Barber, S. Y. Chan, et al. 2003. The genome sequence of the SARS-associated coronavirus. *Science* 300: 1399–1404.

3. Ni, L., F. Ye, M. L. Cheng, Y. Feng, Y. Q. Deng, H. Zhao, P. Wei, J. Ge, M. Gou, X. Li, et al. 2020. Detection of SARS-CoV-2-specific humoral and cellular immunity in COVID-19 convalescent individuals. *Immunity* 52: 971–977.e3.
4. Zhang, Q., P. Bastard, Z. Liu, J. Le Pen, M. Moncada-Velez, J. Chen, M. Ogishi, I. K. D. Sabli, S. Hodeib, C. Korol, et al.; COVID-STORM Clinicians; COVID Clinicians; Imagine COVID Group; French COVID Cohort Study Group; CoV-Contact Cohort; Amsterdam UMC Covid-19 Biobank; COVID Human Genetic Effort; NIAID-USUHS/TAGC COVID Immunity Group. 2020. Inborn errors of type I IFN immunity in patients with life-threatening COVID-19. *Science* 370: eabd4570.
5. Bastard, P., L. B. Rosen, Q. Zhang, E. Michailidis, H. H. Hoffmann, Y. Zhang, K. Dorgham, Q. Philippot, J. Rosain, V. Béziat, et al.; HGID Lab; NIAID-USUHS Immune Response to COVID Group; COVID Clinicians; COVID-STORM Clinicians; Imagine COVID Group; French COVID Cohort Study Group; Milieu Intérieur Consortium; CoV-Contact Cohort; Amsterdam UMC Covid-19 Biobank; COVID Human Genetic Effort. 2020. Autoantibodies against type I IFNs in patients with life-threatening COVID-19. *Science* 370: eabd4585.
6. Akira, S., S. Uematsu, and O. Takeuchi. 2006. Pathogen recognition and innate immunity. *Cell* 124: 783–801.
7. Alexopoulou, L., A. C. Holt, R. Medzhitov, and R. A. Flavell. 2001. Recognition of double-stranded RNA and activation of NF-κB by Toll-like receptor 3. *Nature* 413: 732–738.
8. Fitzgerald, K. A., S. M. McWhirter, K. L. Faia, D. C. Rowe, E. Latz, D. T. Golenbock, A. J. Coyle, S. M. Liao, and T. Maniatis. 2003. IKKε and TBK1 are essential components of the IRF3 signaling pathway. *Nat. Immunol.* 4: 491–496.
9. Rehwinkel, J., and M. U. Gack. 2020. RIG-I-like receptors: their regulation and roles in RNA sensing. *Nat. Rev. Immunol.* 20: 537–551.
10. Yan, N., and Z. J. Chen. 2012. Intrinsic antiviral immunity. *Nat. Immunol.* 13: 214–222.
11. Moustaqil, M., E. Ollivier, H. Chiu, S. V. Tol, P. Rudolffi-Soto, C. Stevens, A. Bhumkar, D. J. B. Hunter, A. N. Freiberg, D. Jacques, et al. 2021. SARS-CoV-2 proteases PLpro and 3CLpro cleave IRF3 and critical modulators of inflammatory pathways (NLRP12 and TAB1): implications for disease presentation across species. *Emerg. Microbes Infect.* 10: 178–195.
12. Shin, D., R. Mukherjee, D. Grewe, D. Bojkova, K. Baek, A. Bhattacharya, L. Schulz, M. Widera, A. R. Mehdipour, G. Tascher, et al. 2020. Papain-like protease regulates SARS-CoV-2 viral spread and innate immunity. *Nature* 587: 657–662.
13. Lei, X., X. Dong, R. Ma, W. Wang, X. Xiao, Z. Tian, C. Wang, Y. Wang, L. Li, L. Ren, et al. 2020. Activation and evasion of type I interferon responses by SARS-CoV-2. *Nat. Commun.* 11: 3810.
14. Miorin, L., T. Kehrer, M. T. Sanchez-Aparicio, K. Zhang, P. Cohen, R. S. Patel, A. Cupic, T. Makio, M. Mei, E. Moreno, et al. 2020. SARS-CoV-2 Orf6 hijacks Nup98 to block STAT nuclear import and antagonize interferon signaling. *Proc. Natl. Acad. Sci. USA* 117: 28344–28354.
15. Zheng, Y., M. W. Zhuang, L. Han, J. Zhang, M. L. Nan, P. Zhan, D. Kang, X. Liu, C. Gao, and P. H. Wang. 2020. Severe acute respiratory syndrome coronavirus 2 (SARS-CoV-2) membrane (M) protein inhibits type I and III interferon production by targeting RIG-I/MDA-5 signaling. *Signal Transduct. Target. Ther.* 5: 299.
16. Tidu, A., A. Janvier, L. Schaeffer, P. Sosnowski, L. Kuhn, P. Hammann, E. Westhof, G. Eriani, and F. Martin. 2020. The viral protein NSP1 acts as a ribosome gatekeeper for shutting down host translation and fostering SARS-CoV-2 translation. *RNA* 27: 253–264.
17. Chen, K., F. Xiao, D. Hu, W. Ge, M. Tian, W. Wang, P. Pan, K. Wu, and J. Wu. 2020. SARS-CoV-2 nucleocapsid protein interacts with RIG-I and represses RIG-mediated IFN-β production. *Viruses* 13: 47.
18. Choi, Y., J. W. Bowman, and J. U. Jung. 2018. Autophagy during viral infection—a double-edged sword. *Nat. Rev. Microbiol.* 16: 341–354.
19. Du, Y., T. Duan, Y. Feng, Q. Liu, M. Lin, J. Cui, and R. F. Wang. 2018. LRRC25 inhibits type I IFN signaling by targeting ISG15-associated RIG-I for autophagic degradation. *EMBO J.* 37: 351–366.
20. Liu, J., X. Wu, H. Wang, J. Wei, Q. Wu, X. Wang, Y. Yan, J. Cui, J. Min, F. Wang, and J. Zhou. 2021. HFE inhibits type I IFNs signaling by targeting the SQSTM1-mediated MAVS autophagic degradation. *Autophagy* 17: 1962–1977.
21. He, X., Y. Zhu, Y. Zhang, Y. Geng, J. Gong, J. Geng, P. Zhang, X. Zhang, N. Liu, Y. Peng, et al. 2019. RNF34 functions in immunity and selective mitophagy by targeting MAVS for autophagic degradation. *EMBO J.* 38: e100978.
22. Wu, Y., S. Jin, Q. Liu, Y. Zhang, L. Ma, Z. Zhao, S. Yang, Y. Li, and J. Cui. 2021. Selective autophagy controls the stability of transcription factor IRF3 to balance type I interferon production and immune suppression. *Autophagy* 17: 1379–1392.
23. Gordon, D. E., G. M. Jang, M. Bouhaddou, J. Xu, K. Obernier, K. M. White, M. J. O'Meara, V. V. Rezelj, J. Z. Guo, D. L. Swaney, et al. 2020. A SARS-CoV-2 protein interaction map reveals targets for drug repurposing. *Nature* 583: 459–468.
24. Chen, C., H. Qin, J. Tan, Z. Hu, and L. Zeng. 2020. The role of ubiquitin-proteasome pathway and autophagy-lysosome pathway in cerebral ischemia. *Oxid. Med. Cell. Longev.* 2020: 5457049.
25. Mirza, M. U., and M. Froeyen. 2020. Structural elucidation of SARS-CoV-2 vital proteins: computational methods reveal potential drug candidates against main protease, Nsp12 polymerase and Nsp13 helicase. *J. Pharm. Anal.* 10: 320–328.
26. Blanco-Melo, D., B. E. Nilsson-Payant, W. C. Liu, S. Uhl, D. Hoagland, R. Møller, T. X. Jordan, K. Oishi, M. Panis, D. Sachs, et al. 2020. Imbalanced host response to SARS-CoV-2 drives development of COVID-19. *Cell* 181: 1036–1045.e9.
27. Zhang, Y., H. Sun, R. Pei, B. Mao, Z. Zhao, H. Li, Y. Lin, and K. Lu. 2021. The SARS-CoV-2 protein ORF3a inhibits fusion of autophagosomes with lysosomes. *Cell Discov.* 7: 31.
28. Wang, B., L. Wang, X. Kong, J. Geng, D. Xiao, C. Ma, X. M. Jiang, and P. H. Wang. 2020. Long-term coexistence of SARS-CoV-2 with antibody response in COVID-19 patients. *J. Med. Virol.* 92: 1684–1689.
29. Zhou, Z., L. Ren, L. Zhang, J. Zhong, Y. Xiao, Z. Jia, L. Guo, J. Yang, C. Wang, S. Jiang, et al. 2020. Heightened innate immune responses in the respiratory tract of COVID-19 patients. *Cell Host Microbe* 27: 883–890.e2.
30. Hoagland, D. A., R. Møller, S. A. Uhl, K. Oishi, J. Frere, I. Golynker, S. Horiuchi, M. Panis, D. Blanco-Melo, D. Sachs, et al. 2021. Leveraging the antiviral type I interferon system as a first line of defense against SARS-CoV-2 pathogenicity. *Immunity* 54: 557–570.e5.
31. Hayn, M., M. Hirschenberger, L. Koepke, R. Nchioua, J. H. Straub, S. Klute, V. Hunszinger, F. Zech, C. Prelli Bozzo, W. Aftab, et al. 2021. Systematic functional analysis of SARS-CoV-2 proteins uncovers viral innate immune antagonists and remaining vulnerabilities. *Cell Rep.* 35: 109126.
32. Vazquez, C., S. E. Swanson, S. G. Negatu, M. Dittmar, J. Miller, H. R. Ramage, S. Cherry, and K. A. Jurado. 2021. SARS-CoV-2 viral proteins NSP1 and NSP13 inhibit interferon activation through distinct mechanisms. *PLoS One* 16: e0253089.
33. Yuen, C. K., J. Y. Lam, W. M. Wong, L. F. Mak, X. Wang, H. Chu, J. P. Cai, D. Y. Jin, K. K. To, J. F. Chan, et al. 2020. SARS-CoV-2 nsp13, nsp14, nsp15 and orf6 function as potent interferon antagonists. *Emerg. Microbes Infect.* 9: 1418–1428.
34. Zhang, K., Y. Zhang, J. Xue, Q. Meng, H. Liu, C. Bi, C. Li, L. Hu, H. Yu, T. Xiong, et al. 2019. DDX19 inhibits type I interferon production by disrupting TBK1-IKKε-IRF3 interactions and promoting TBK1 and IKKε degradation. *Cell Rep.* 26: 1258–1272.e4.
35. Cui, J., Y. Li, L. Zhu, D. Liu, Z. Songyang, H. Y. Wang, and R. F. Wang. 2012. NLRP4 negatively regulates type I interferon signaling by targeting the kinase TBK1 for degradation via the ubiquitin ligase DTX4. *Nat. Immunol.* 13: 387–395.
36. Zhang, M., L. Wang, X. Zhao, K. Zhao, H. Meng, W. Zhao, and C. Gao. 2012. TRAF-interacting protein (TRIP) negatively regulates IFN-β production and antiviral response by promoting proteasomal degradation of TANK-binding kinase 1. *J. Exp. Med.* 209: 1703–1711.
37. Friedman, C. S., M. A. O'Donnell, D. Legarda-Addison, A. Ng, W. B. Cárdenas, J. S. Yount, T. M. Moran, C. F. Basler, A. Komuro, C. M. Horvath, et al. 2008. The tumour suppressor CYLD is a negative regulator of RIG-I-mediated antiviral response. *EMBO Rep.* 9: 930–936.
38. Zhang, L., X. Zhao, M. Zhang, W. Zhao, and C. Gao. 2014. Ubiquitin-specific protease 2b negatively regulates IFN-β production and antiviral activity by targeting TANK-binding kinase 1. *J. Immunol.* 193: 2230–2237.
39. Huang, L., H. Liu, K. Zhang, Q. Meng, L. Hu, Y. Zhang, Z. Xiang, J. Li, Y. Yang, Y. Chen, et al. 2020. Ubiquitin-conjugating enzyme 2S enhances viral replication by inhibiting type I IFN production through recruiting USP15 to deubiquitinate TBK1. *Cell Rep.* 32: 108044.
40. Song, G., B. Liu, Z. Li, H. Wu, P. Wang, K. Zhao, G. Jiang, L. Zhang, and C. Gao. 2016. E3 ubiquitin ligase RNF128 promotes innate antiviral immunity through K63-linked ubiquitination of TBK1. *Nat. Immunol.* 17: 1342–1351.
41. Li, S., L. Wang, M. Berman, Y. Y. Kong, and M. E. Dorf. 2011. Mapping a dynamic innate immunity protein interaction network regulating type I interferon production. *Immunity* 35: 426–440.
42. Wang, C., T. Chen, J. Zhang, M. Yang, N. Li, X. Xu, and X. Cao. 2009. The E3 ubiquitin ligase Nrdp1 "preferentially" promotes TLR-mediated production of type I interferon. *Nat. Immunol.* 10: 744–752.
43. You, H., S. Zheng, Z. Huang, Y. Lin, Q. Shen, and C. Zheng. 2019. Herpes simplex virus 1 tegument protein UL46 inhibits TANK-binding kinase 1-mediated signaling. *MBio* 10: e00919-19.
44. Sui, L., Y. Zhao, W. Wang, P. Wu, Z. Wang, Y. Yu, Z. Hou, G. Tan, and Q. Liu. 2021. SARS-CoV-2 membrane protein inhibits type I interferon production through ubiquitin-mediated degradation of TBK1. *Front. Immunol.* 12: 662989.
45. White, M. A., W. Lin, and X. Cheng. 2020. Discovery of COVID-19 inhibitors targeting the SARS-CoV-2 Nsp13 helicase. *J. Phys. Chem. Lett.* 11: 9144–9151.
46. Liu, T., Q. Tang, K. Liu, W. Xie, X. Liu, H. Wang, R. F. Wang, and J. Cui. 2016. TRIM11 suppresses AIM2 inflammasome by degrading AIM2 via p62-dependent selective autophagy. *Cell Rep.* 16: 1988–2002.
47. Prabakaran, T., C. Bodda, C. Krapp, B. C. Zhang, M. H. Christensen, C. Sun, L. Reinert, Y. Cai, S. B. Jensen, M. K. Skouboe, et al. 2018. Attenuation of cGAS-STING signaling is mediated by a p62/SQSTM1-dependent autophagy pathway activated by TBK1. *EMBO J.* 37: e97858.